Oldest (ca. 518 Ma) Mariana type oceanic subduction initiation ophiolite: constraining initiation of modern oceanic plate tectonic regime

Jinlong Yao (yaojinlong@nwu.edu.cn)
Northwest University
Peter Cawood
Monash University https://orcid.org/0000-0003-1200-3826
Guochun Zhao
The University of Hong Kong
Yigui Han
Northwest University
Xiao-Ping Xia
State Key Laboratory of Isotope Geochemistry, Guangzhou Institute of Geochemistry, Chinese Academy of Sciences, Guangzhou 510640, China https://orcid.org/0000-0002-3203-039X
Qian Liu
The University of Tsukuba
Peng Wang
The University of Hong Kong

Article

Keywords: subduction initiation ophiolite, northern Tibet, chemical duality, Zircon Hf-O isotopes and H2O contents, Proto-Tethys Ocean, modern plate tectonic regime

Posted Date: March 10th, 2021

DOI: https://doi.org/10.21203/rs.3.rs-287716/v1

Version of Record: A version of this preprint was published at Nature Communications on July 7th, 2021. See the published version at https://doi.org/10.1038/s41467-021-24422-z.

Abstract

Initiation of stable Mariana type one-sided oceanic subduction zones requires rheologically strong oceanic lithosphere, which developed through secular cooling of Earth mantle. This enabled the development of focused high stress zones resulting in narrow weak zones of convergence with resultant oceanic subduction leading to mantle hydration and arc magmatism. Based on detailed study and identification of the oldest (518 Ma) Mariana type oceanic subduction initiation ophiolite (Munabulake ophiolite) on Earth from northern Tibet, along with compilation of oceanic subduction initiation ophiolites through Earth history, we argue for the initiation of modern plate tectonic regime by at least the early Cambrian. The mantle and crust members of the Munabulake ophiolite preserve a complete ophiolite stratigraphy. Blocks of layered marble and siliceous rocks interlayered with meta-basalt indicate a marine environment. Zircons from an olivine gabbro sample yield a concordant age of 518 Ma, along with mantle derived low $\delta^{18}O$ (2.69‰ – 5.7‰) and high εHf(t) (11.1–13.6) values. The zircons also have varied H_2O contents ranging from 109–1339 ppm with peaks at 260 and 520 ppm, indicative of hydration of mantle derived magma. The highly depleted peridotites display U–shaped REE patterns and varied Zr/Hf ratios, whereas spinel and olivine compositions within the peridotites indicate that they are residues of various degrees of melt extraction and evolved from abyssal to fore-arc peridotites. The crustal members of the ophiolite are mostly tholeiitic, display flat REE patterns and lower HFSEs, comparable to transitional lavas associated with Mariana subduction initiation ophiolite. Some rocks from the crustal section of the ophiolite display NMORB-like compositions but are also characterized by depletion in HSFEs. Therefore, the Munabulake ophiolite displays a chemical duality and progressively evolved from MORB (mid-ocean ridge basalt) to SSZ (supra-subduction zone) compositions, consistent with observations from zircon Hf-O isotopes and H_2O contents. Furthermore, the ophiolite was formed during subduction initiation of the Proto-Tethys Ocean at the northern Gondwana margin, and coincided with an inferred slab roll back event in the southern Gondwana margin at ca. 530 – 520 Ma, indicative of a time of global tectonic re-organization. The early Cambrian Munabulake ophiolite indicates comparable slab strength and conditions to those that characterize modern plate tectonics. Such a tectonic regime coincided with final Gondwana assembly, and was associated with ca. 530 – 520 Ma global tectonic re-organization.

Introduction

The commencement and evolution of the plate tectonic regime on Earth is linked to secular mantle cooling and associated increasing lithospheric strength (1-4). Some form of plate tectonics is generally inferred to have initiated in the late Archean, as mantle potential temperature dropped below ΔT = 250 °C (relative to present-day values) and lithosphere strength increased (4-5). In the Neoproterozoic-Cambrian, during Gondwana assembly, mantle temperature dropped below ΔT = 80-100 °C, lithosphere strength further increased, enabling deep plate subduction and corresponding with the widespread record of high P/T UHP metamorphic assemblages, and is accepted as the start of a plate tectonic regime that

continues to the present day (1, 6-7). This period also marks significant changes in surficial climate and biosphere, marking the beginning of the contemporary Earth (8 and references therein).

Subduction initiation is a key component of the plate tectonic paradigm and results in the closing of ocean basins, culminating in arc-continent and continent collisions, and exerts a major control on the modern Earth system through exchange between surficial and solid Earth reservoirs (9). Key factors in the initiation of a stable modern, Mariana type, intra-oceanic subduction zone includes high slab strength, weak zones of focused stress, and mantle wedge hydration (2). It is characterized by the formation of a proto-arc ophiolite (also referred to as a subduction initiation ophiolite), subsequently preserved in the fore-arc of the resultant convergent plate margin, and contains boninites, basalts, gabbroic rocks, and mantle peridotites (10-12). The igneous sequences are derived from mantle sources that evolved from the combined effects of melt depletion and subduction-related metasomatism, and form within 7-10 Ma of subduction initiation (11-13). Ophiolites that form at the initiation of subduction are, however, rarely preserved (12). Examples include the Izu-Bonin-Mariana ophiolite (11, 14), the late Cretaceous Tethyan ophiolites (13, 15), the early Carboniferous Paleo-Asian Ocean ophiolite (16), and the early Ordovician Appalachian-Caledonian ophiolites (17-18).

In this paper, we document the ca. 518 Ma Munabulake ophiolite from the Southern Altyn Terrane (also referred to as the Southern Altyn HP-UHP belt) in northern Tibet. Ophiolite stratigraphy, field relations, ages, zircon Hf-O isotopes and H_2O compositions, along with whole rock and mineral compositions argue for formation during intra-oceanic subduction initiation. This ophiolite is the oldest ophiolite formed during initiation of Mariana type oceanic subduction in Earth history, which we link to other subduction initiation ophiolites in Earth history and argue for high oceanic slab strength and initiation of modern plate tectonics at least since early Cambrian. The Munabulake ophiolite is also the first record of the subduction initiation of the Proto-Tethys Ocean at the northern Gondwana margin (19-21), and coincides with a period of global tectonic re-organization.

Geological background

The Tarim Block lies between the Central Asian Orogenic Belt (CAOB) and the Tibetan Plateau (Fig. 1a). The block is largely covered by desert but Precambrian rocks are exposed around its margins (22-24), and its southern margin is marked by the early Paleozoic Kunlun and Altyn orogenic belts (Fig. 1a, 25-29).

The Altyn Belt records multiple orogenic cycles, including Archean-Paleoproterozoic and latest Mesoproterozoic-Neoproterozoic events that were extensively overprinted in the early Paleozoic (24, 28-31). Its northern boundary is the northern Altyn fault zone, but its southern margin is less well constrained and is offset by the Cenozoic reactivation of the Altyn fault zone associated with India-Asia collision (Fig. 1a, 26, 31). The Altyn Belt is divisible into three Precambrian-early Paleozoic continental terranes (the north, central and south Altyn terranes) and two early Paleozoic ophiolite belts (the Hongliugou-Lapeiquan and southern Altyn ophiolitic belts) (Fig. 1a). The Hongliugou-Lapeiquan belt delineates the boundary between the north and central Altyn terranes, whereas the southern Altyn ophiolitic belt is

located at the southeastern margin of the South Altyn Terrane (Fig. 1a). The boundary between central and south Altyn terranes is inferred to be an unnamed strike slip fault (Fig. 1a).

The North Altyn Terrane contains an assemblage of Archean to Paleoproterozoic igneous and metamorphic rocks which are considered to constitute the basement to the Tarim Block, and are unconformably overlain by Mesoproterozoic strata (24, 32). **The central Altyn Terrane**, also referred to as the Milanhe-Jinyanshan terrane, is dominated by marble and meta- clastic sedimentary rocks that are covered by a thick layer of limestone-dolomite, both assigned to the Mesoproterozoic Jixian system, but latest investigations suggest Neoproterozoic to early Paleozoic ages (author unpublished data, 33). The units are unconformably overlain by limestone and clastic sedimentary rocks of the early Paleozoic Suoerkuli Group. Voluminous early Paleozoic granitoids dated at 522-430 Ma, mostly S-type, intrude into these sequences (34-35). Meta-mafic arc sequences dated at ca. 520-510 Ma occur within the northern margin of the terrane (author unpublished data). **The Southern Altyn Terrane** consists primarily of the Altyn Complex, which consists of a suite of granitic gneisses and meta-sedimentary rocks, including ortho- and paragneisses, marbles, amphibolites, and minor meta-mafic-ultramafic rocks (30, 32). The complex was considered to be Archean-Paleoproterozoic in age (32), but recent works indicate the complex contains latest Mesoproterozoic to early Paleozoic units, which experienced multiple stages of metamorphism and deformation at 500-430 Ma, as well as events at, or after, ca. 235 Ma (30, 36, author unpublished data). An inferred ophiolitic mélange of early Paleozoic age is also present in the complex. HP-UHP metamorphic rocks occur as lenses within the Altyn Complex, including UHP eclogite and kyanite-garnet bearing pelitic gneiss, HP-UHP garnet lherzolite (27-28). These HP/UHP rocks yield metamorphic ages of ca. 509-475 Ma, with their protolith constrained to ca. 840-750 Ma (27). Granitic plutons with variable compositions (I-, S- and A- types) intrude into the Altyn Complex. Limited dating on these intrusions yield ages of 462-440 Ma (e.g. 34-37).

The southern Altyn ophiolite belt and the Hongliugou-Lapeiquan ophiolite belt are inferred to be fragments of the Proto-Tethys Ocean (20, 28). Some recent work suggests these ophiolites were part of a single subduction zone repeated by oroclinal bending (20). **The Hongliugou-Lapeiquan ophiolitic belt** consists mainly of sheared and deformed ophiolitic rock units of both supra-subduction zone (SSZ) and mid-ocean ridge basalt (MORB) affinities, and are dated at 518 ± 4 Ma, 513 ± 3 Ma, and 479 ± 8 Ma (SHRIMP zircon U-Pb and LA-ICP-MS zircon U-Pb; 38-39). Ophiolite components include serpentinized harzburgite and lherzolite, mafic-ultramafic cumulates, sheeted dykes, and pillow basalt (38). **The South Altyn ophiolite belt**, extending more than 700 km along strike from Mangya to Tula lies within the Altyn fault zone and contains ophiolite mélange and flysch. The sheared ophiolite sequences are not well preserved and occur as disrupted blocks of serpentinized dunite, harzburgite and some gabbroic rock, dated at 510 ± 1 and 501 ± 2 Ma (37 and references therein). Ca. 517 Ma and 503 Ma adakite also occurs within this ophiolite belt (e.g. 37 and references therein).

Stratigraphy of the Munabulake ophiolite in the South Altyn Terrane and sampling

The Munabulake ophiolite, occurs as a tectonic block within the Altyn Complex in the South Altyn Terrane (32). It was extensively sheared and deformed into an overall diamond shape. The ophiolite is thrust upon other units of the complex at its northern margin, whereas on its southwestern margin, a NW-SE directed sinistral strike slip ductile shear zone delineates the boundary with the remainder of the Altyn Complex (Fig. 1b, 1c). Original contacts between units within the complex remain unclear as they experienced long-term high-grade metamorphism and extensive deformation at ca. 500-420 Ma and in the early Mesozoic (27, 31).

From southwest to northeast, and corresponding with the progression from base to top, the Munabulake ophiolite is composed of sheared serpentinite along the basal thrust, serpentinized dunite-harzburgite, pyroxene peridotite, olivine pyroxenite, gabbro, and meta-basaltic and meta-intermediate igneous suites, along with blocks of marble (Fig. 1b, 2a, 2b). Fine grained siliceous rocks ranging in size from centimeters to meters thick are interlayered with the basaltic and intermediate igneous suites (Figs. 2c). They are interpreted to represent recrystallized chert and are indicative of a deep-sea marine environment. This is consistent with layered marbles that are also present in some localities (Fig. 2d). Ultramafic blocks of serpentinized dunite and pyroxene peridotite, up to 7 km thick, are exposed in the northwest segment of the ophiolite (Fig. 1b, 1c, 2b). An olivine pyroxenite block, approximately 2 km thick, also occurs between blocks of serpentinized dunite and pyroxene peridotite, whereas a harzburgite block is sandwiched between blocks of serpentinized dunite (Fig. 1b). The ultramafic rocks, generally serpentinized, are interpreted as the lower mantle components of the ophiolite. A structural block that consists mainly of meta-gabbro and meta- basaltic-intermediate suites occurs within the ductile shear zone along the southwest margin of the ophiolite (Fig. 1b, 2e). Pillow basalt, along with deep sea turbidites form the upper crustal components of the ophiolite stratigraphy (32), but diabase dikes are less developed. These suites form the crustal member of the ophiolite. In summary, the overall lithological assemblage is consistent with a disrupted ophiolite, and occurs within gneisses of the Altyn Complex. 4 peridotite samples and 17 basaltic-intermediate samples are selected from the ophiolite for Zircon U-Pb ages, Hf-O isotopes and H_2O contents, along with whole rock and mineral compositions. Detailed analytic procedures and results can be found in supplementary text and tables.

Results

Zircons from the meta-gabbro are euhedral grains and show banded zones in CL images, comparable to zircons crystallized from mafic magmas (Fig. 3). Thin metamorphic rims are visible but are too narrow for U-Pb age analyses (Fig. 3). The analyzed grains display Th/U ratios of 0.5-3.0 (Table S1), which are comparable to those of magmatic zircons. Forty-two analyses from the meta-gabbro sample 17SAT13-2 yielded a concordant $^{206}Pb/^{238}U$ age range of 543–506 Ma and a weighted mean age of 518 ± 2 Ma (MSWD = 0.94, n = 40) (Fig. 3).

Zircon grains from meta-gabbro sample 17SAT13-2 display present day $^{176}Hf/^{177}Hf$ ratios of 0.282792–0.282863, equivalent to εHf(t) values of 11.1–13.6 and Hf model ages of 566–670 Ma (Fig. 4a). Zircon grains from this sample also have $\delta^{18}O$ compositions of +2.69 ‰ – +5.7 ‰ (Fig. 4b) that are

comparable to, and lower than, mantle zircons (40). Thus, zircon Hf-O isotopes argue for crystallization of zircon grains from mantle derived mafic magmas. In addition, H_2O-in-zircon contents of these grains range between 109 ppmw and 1339 ppmw, with two peaks at 260 and 520 ppmw. No obvious correlation between zircon δ18O values and H2O contents has been observed (Fig. 4b).

This study focuses on the immobile elements and element ratios, considering the potential for mobilization of large ionic radius elements during metamorphism and alteration. In addition, oxides in this study were recalculated on an anhydrous (volatile-free) basis, with the oxide sum normalized to 100 %.

The meta-mafic samples display a wide compositional range with SiO_2 of 45.96–52.22 wt.%, MgO of 4.75-9.91 wt.%, TiO_2 of 0.1–1.08 wt.%, and Mg# of 43–75. These samples display almost flat rare earth element (REE) patterns, with no obvious Ce and Eu anomalies. They exhibit relative depletions in high field strength elements (HFSE), such as Nb and Ta (Fig. 5a, 5b). Two basaltic samples also display both LREE and HFSE depletions, whereas the gabbro sample shows minor flat light rare earth element (LREE) enrichment (Fig. 5c, 5d). The meta-intermediate samples are characterized by SiO_2 of 52.98–57.32 wt.%, MgO of 3.66-5.17 wt.%, and mostly flat REE patterns and variable depletions in HFSEs such as Nb and Ta (Fig. 5a, 5b). Most of the meta-basaltic and meta-intermediate samples belong to the tholeiitic series. The ultramafic samples display a very low compositional range for TiO_2 (0.1–0.09 wt.%), SiO_2 (32.48–44.83 wt.%), but very high MgO (42.32-46.27 wt.%) and Mg# of 90–92. They display overall low REE contents (mostly 0.48-11.6 ppm), slight LREE enrichment and U-shaped REE patterns, with minor Nb and Ta depletions (Fig. 5c, 5d).

Less serpentinized harzburgite samples 17SAT22-1 and 18SAT41-4 and olivine pyroxenite sample 18SAT41-5 were selected for olivine and spinel compositional analyses (Fig. 2f). The olivines display a uniform composition (Fig. 6) and in the pyroxenite has Fo values of 90.9–91.7 and NiO contents of 0.256–0.524 wt.%, whereas in the harzburgite shows Fo values between 89.9 and 91.9, and NiO contents of 0.25 and 0.46 wt.% (Fig. 6b). Peridotites spinels are resistant to secondary alteration processes and preserve environmental records of peridotites formation (reference). Oxidized rims can be observed in some spinels, so analyses were only undertaken on fresh cores. The analyzed spinels display a wide compositional range. The Cr# values of spines in the olivine pyroxenite (26–77) are lower than depleted harzburgite (71-84) and a linear trend of Cr# vs Mg# values for spinels can also be observed (Fig. 6c). TiO_2 contents are lower in the olivine pyroxenite (0-0.14 wt.%) than those in the harzburgites (0.11-0.20 wt.%) (Fig. 6d), whereas the NiO contents display a decrease from olivine pyroxenite to harzburgite.

Chemical duality of the Munabulake ophiolite: progressive evolution from MORB to SSZ compost ions during intra-oceanic subduction initiation

The mantle members of the Munabulake ophiolite consists of residual dunite, harzburgite, and olivine pyroxenite (Fig. 1b). The negatively correlated Cr# vs Mg# values of spinels within harzburgite and olivine pyroxenite samples suggest that the investigated rocks represent residual mantle, with the olivine

pyroxenite related to low degrees of partial melting and melt extraction and the harzburgite to higher degrees (Fig. 6b). The correlation between Mg# values of olivines and the Cr# values of spinels is conformable with the olivine–spinel mantle array (Fig. 6c), also indicating the peridotite samples are residues of various degrees of melt extraction. Spinel TiO_2 vs Cr# trend suggests a similar magma process (Fig. 6d). The studied residue ultramafic samples have higher Mg# (> 90) values than primitive mantle, and also display U–shaped REE patterns and that are indicative of melt introduction (Fig. 5c), consistent with high flux and volatile conditions in a supra-subduction zone setting. Melt or fluid metasomatism can also be observed from tremolite and enclosure of olivine grains in orthopyroxene in peridotite, as are their varied Zr/Hf ratios. The magma evolution thus reflects progressive source depletion coupled with increasing melt or fluid metasomatism. Therefore, compositions of ultramafic rocks and spinel-olivine minerals are consistent with progressive chemical evolution from abyssal to arc-related peridotite (Fig. 6).

The meta-basaltic and intermediate samples from the Munabulake ophiolite have high MgO contents (5.12-9.95 wt.% for mafic samples and 3.54-5.27 wt.% for intermediate samples), low TiO_2 (< 1 wt.%), mostly flat REE patterns, along with obvious depletions of Nb and Ta, and very minor Ti depletions for some samples. LREE depleted patterns are also observed in two samples. In addition, the investigated mafic-intermediate samples are characterized by elevated Th in the Nb/Yb vs. Th/Yb diagram (Fig. S1a), where most of the samples lie above the mantle array, indicating Th enrichment in their mantle source, which is consistent with fluid flux melting and was likely derived from subducted slab sediment. Moreover, U/Th-Th/Nb and Ba/Th-La/Sm diagrams (not shown) also favor involvement of hydrous fluids from altered oceanic crust. This chemical evolution trend indicates increasing source metasomatism by slab-derived material (elevating Th, U, and some LREE).

The analyzed samples plot in the SSZ type ophiolite field in various tectonic discrimination diagrams, including Ta/Yb vs. Th/Yb and Ti vs. V (Fig. S1c). Their lower TiO2 (< 1.25 wt. %), Zr/Y (< 3), Nb/La (< 0.5), Hf/Th (mostly < 2), and Ta/Yb (< 0.1), along with higher Th/Nb (> 0.2) and Th/Yb (> 0.1) (Table S2), are comparable to those of oceanic arc basalts (41). Although these compositional features indicate metasomatism by a subducted slab, their flat REE patterns argue against an island arc setting (Fig. 5a), as do their mostly tholeiitic compositions. In addition, even compared to lavas of nascent oceanic island arcs such as Saipan-Rota-Guam (42), the investigated mafic-intermediate samples lack marked Eu and Ti anomalies (Fig. 5b). This indicates no plagioclase fractionation and very minor rutile fractionation. These signatures suggest that no normal arc or felsic crust had formed at the time of ophiolite formation. In addition, the higher Y/Zr values of these igneous rocks argue for derivation from depleted mantle source (11), whereas Hf/Nb versus Zr/Nb suggests magma enrichment by subducted fluids (43). The overall chemical signatures and evolution trends are comparable to crustal members of the IBM and Tethyan ophiolites (Fig. 5, S1; 13-14), consistent with the observations from Munabulake mantle end-members. More importantly, H_2O contents in mantle zircons within the ophiolitic gabbro indicate similar processes, with two populations at 160-320 ppmw and 480-640 ppmw (Fig. 4b). The zircons with low H_2O content are comparable to MORB zircons (44), whereas the zircons with higher water content indicate possible

progressive magma hydration due to formation of a subduction zone. In addition to the mantle zircons in the ophiolite, zircons with lower $\delta^{18}O$ isotopes (+2.69 ‰ – +5.0 ‰, peaked at 4.7‰) are also observed, which are comparable to altered oceanic crust (45). All the observations suggest linkages between progressive source depletion and metasomatism due to slab-derived fluids, which is commonly expected for a subduction initiation ophiolite and is consistent with observations from mantle end-members. However, it is noteworthy that the mafic-intermediate units occur within a ductile shearing zone and were subjected to multi-stage higher grade metamorphism and shearing. Thus, detailed reconstruction of overall chemo-stratigraphy is difficult.

Direct record of the oldest oceanic subduction initiation at ca. 518 Ma

The south Altyn margin is characterized by the following: 1) Munabulake ophiolite dated at 518 Ma; 2) the 508-475 Ma UHP-HP metamorphism (27); 3) ca. 508-505 Ma arc related magmatism at a few localities to the north of the Munabulake ophiolite (author unpublished data); 4) ca. 510-500 Ma MORB type mafic-ultramafic rocks and ca. 503 Ma adakite-diorite (Fig. 5e, 5f, 5g, 5h, S1a; 37 and reference therein); 5) ca. 517 Ma oceanic type adakite, along with calc-alkaline granitoids dated at ca. 503–497 Ma occurring in various localities (Fig. 5g, 5h, S1a; e.g. 34-38); and, 6) sinistral shearing along the fault zone at southern margin of the Munabulake ophiolite sometime after ca. 235 Ma (Fig. 1b) (26, 31).

The overall ages and field relations indicate that the 518 Ma Munabulake ophiolite is the oldest oceanic succession in the Southern Altyn, followed by establishment of an intra-oceanic arc system lasting some 20 Ma at least until ca. 500 Ma, as is inferred from the 510-500 Ma MORB type mafic-ultramafic suites and ca. 503–497 Ma arc type granitoids and adakite-diorite. Thus, the crustal and mantle members of the Munabulake ophiolite, along with available data across the south Altyn, agree with the subduction initiation signature of the 518 Ma ophiolite, which we conclude to be have been formed during subduction initiation of the Proto-Tethys Ocean, in a scenario similar to the IBM ophiolites (Fig. S1). The reported ca. 517 Ma oceanic type adakite was generated by partial melting of oceanic crust in a newly formed subduction zone. Moreover, given the large-scale sinistral shearing of the south Altyn fault zone, we infer that the Munabulake ophiolite should be a member of the south Altyn ophiolite belt and was offset to current location by strike-slip motion of the fault system.

Global plate re-organization at ca. 530-520 Ma during Gondwana assembly

The Munabulake ophiolite dates the subduction initiation of the Proto-Tethys Ocean in the Altyn segment, but the overall subduction initiation of this ocean is not well constrained and earlier inferred individual subduction zones have largely been treated in isolation (e.g., 19, 21, 25, 28, 46-47). In addition, the ocean has been given a number of localized names adjacent to the variety of continental and arc related blocks in East Asia that are inferred to lie within the ocean. The early Paleozoic oceanic successions in these blocks are related to the evolution of the ocean and accretion of these blocks to the northern Gondwana margin (e.g., 19-21, 47). Nevertheless, here in this study, a time-space plot of early Paleozoic ophiolites and trench-arc assemblages across East Asia blocks, along with related magmatic and metamorphic

events, enables determination of overall timing of initial oceanic subduction of the Proto-Tethys Ocean (Fig. 7). In particular, elsewhere across East Asia, ages of initiation of subduction are inferred from the oldest arc magmatism, which are in accordance with stratigraphy and ages of ophiolite and metamorphic event (Fig. 7). We conclude that the main branch of the Proto-Tethys Ocean principally subducted northward and commenced at ca. 533 Ma in the West Kunlun segment (25-26), at ca. 525-520 Ma in the Altyn-Qaidam-Qilian segments (28, 46; this study), and at ca. 515 Ma in the North Qinling segment (Fig. 7, 8; 47). Locally, possible isolated subduction zones in the Qiangtang and Indochina segments commenced at sometime around 535 Ma and 490 Ma (19, 21, 49), but these dates are not well constrained. Therefore, overall timing of oceanic subduction initiation of the Proto-Tethys Ocean displays an eastward younging direction from ca. 533 Ma in the west segment to ca. 515 Ma in the east most segment.

It is noteworthy that the timing of initial subduction of the Proto-Tethys Ocean coincides well with the timing of slab roll-back of the Pacific Ocean in the southern Gondwana margin (50) (Fig. 8). The extension regime in the southern Gondwana and expression regime in the northern Gondwana was thus strictly correlated, indicative of global plate re-organization at this time, which is linked to final collisional assembly of Gondwana.

Subduction initiation ophiolites in Earth history: initiation of modern plate tectonic regime

Ophiolites formed during simultaneous subduction initiation of a modern Mariana type oceanic subduction zone include the 52 Ma Izu-Bonin-Mariana ophiolites and Tonga ophiolite in west Pacific (9, 11-12, 14), 100-90 Ma Tethyan ophiolites (13, 15), the ca. 335 Ma Paleo-Asian Ocean ophiolite (16), 490-485 Ma Appalachian-Caledonian ophiolites (17-18), and the 518 Ma Munabulake ophiolite (Proto-Tethys ophiolite) in northern Gondwana margin in this study (Fig. 8). Given the conditions required for simultaneous initiation of stable one-sided modern Mariana type oceanic subduction (2), the key factors of oceanic plate tectonic regime, slab strength in particular, must have been comparable at least since the early Cambrian time. This was controlled by progressive cooling of mantle which increased slab strength (3, 51). High slab strength, along with comparable ophiolite characteristics and scenarios of simultaneous oceanic subduction initiation since the early Cambrian, coincides well with the inferred transition from early plate tectonic regime to modern plate tectonic regime in the Neoproterozoic-Cambrian (7, 52). Earlier conclusions on the transition of tectonic regime in the Neoproterozoic- Cambrian are mostly based on records of the Phanerozoic low T/P UHP metamorphic rocks and geodynamic modelling results that indicate drops of mantle temperatures below ΔT= 80-100°C at this time (Fig. 9), and thus plate strength was strong enough for deep plate subduction (1, 6). On the other hand, the subduction initiation ophiolites discussed in this study also argue for modern plate tectonics at least since the earliest Phanerozoic, consistent with significant drops of mean thermobaric ratios at 525 Ma (Fig. 9). In addition, recent works also favor formation of Earth inner core in the Ediacaran (53), which might have feedback effects on plate tectonic regime. We suggest that following the global plate re-organization at ca. 530-520 Ma during Gondwana assembly, a plate tectonic regime with products and slab strength similar to modern day Earth was achieved.

Conclusion

The disrupted and sheared stratigraphy in the Munabulake area of the south Altyn Terrane comprises a disrupted ophiolite with mantle related components of residual peridotites and crustal components of meta-mafic and intermediate igneous suites. The ophiolite is interpreted as formed during the initiation of subduction of the Proto-Tethys Ocean in the northern Gondwana margin and is dated at ca. 518 Ma. Varied siliceous layers within mafic lavas and blocks of layered marble establish a deep marine environment. Geochemical, isotopic, and mineral compositional data constrains a chemical duality, with progressive evolution from MORB to SSZ and is analogous to the Mariana subduction initiation ophiolite. The Munabulake ophiolite is the oldest simultaneous subduction initiation ophiolite on Earth and corresponded to a period of global tectonic reorganization in Gondwana margins. Overall distributions and formation conditions of subduction initiation ophiolites on Earth argue for a modern type oceanic plate tectonic regime at least since the early Cambrian, and corresponding with final Gondwana assembly.

Declarations

Data availability

All data generated during this study are included in the supporting information.

Acknowledgement

This research is funded by the NSFC grants (41730213, 41972238 and 41190075), the State Key Laboratory of Continental Dynamics (201212000174) and the Hong Kong Research Grants Council General Research Fund (grants 17306217, 17307918 and 17301915). Peter A. Cawood acknowledges Australian Research Council grant FL160100168 for support. Drs. Ningchao Zhou, Zengchan Dong and Shan Yu are thanked for their help during field work. The manuscript benefited from discussion with Drs. Yunying Zhang, Peiyuan Hu, Dengfeng He, and Anping Chen. We also thank Drs. Jianfeng Gao, Ningchao Zhou and Xing Cui, and Mr. Liang Li for their helps with zircon isotopic and geochemical analyses.

References

1. Brown, M. Metamorphic conditions in orogenic belts: A record of secular change. *International Geology Review* 49. 193–234 (2007).
2. Gerya, T. V., Connolly, J. A., & Yuen, D. A. Why is terrestrial subduction one-sided? *Geology*, *36*(1), 43-46 (2008).
3. Cawood, P.A. & Hawkesworth, C.J. Earth's middle age. *Geology* 42, 503–506 (2014).
4. Cawood, P.A. et al. Geological archive of the onset of plate tectonics. *Philosophical Tansactions of the Royal Society: Series A, Mathematical, Physical, and Engineering Sciences* 376, 2132 (2018).

5. Tang, M., Chen, K., & Rudnick, R. L. (2016). Archean upper crust transition from mafic to felsic marks the onset of plate tectonics. *Science* 351(6271), 372-375.
6. Stern, R.J., Tsujimori, T., Harlow, G. & Groat, L.A. Plate tectonic gemstones. *Geology* 41, 723–726 (2013).
7. Sizova, E., Gerya, T., & Brown, M. (2014). Contrasting styles of Phanerozoic and Precambrian continental collision. *Gondwana Research 25*(2), 522-545.
8. Cawood, P. A. Earth Matters: A tempo to our planet's evolution. *Geology* 48(5), 525-526 (2020).
9. Stern, R. J. & Gerya, T. Subduction initiation in nature and models: A review. *Tectonophysics* 746, 173-198 (2018).
10. Leitch, E.C. Island arc elements and arc-related ophiolites. *Tectonophysics* 106(3-4), 177-203 (1984).
11. Ishizuka, O. et al. The timescales of subduction initiation and subsequent evolution of an oceanic island arc. *Earth and Planetary Science Letters* 306, 229–240 (2011).
12. Stern, R. J. et al. To understand subduction initiation, study forearc crust: To understand forearc crust, study ophiolites. *Lithosphere* 4(6), 469-483 (2012).
13. Whattam, S.A. & Stern, R.J. The 'subduction-initiation rule': A key for linking ophiolites, intra-oceanic forearcs and subduction initiation. *Contributions to Mineralogy and Petrology* 162, 1031–1045 (2011).
14. Reagan, M.K. et al. Fore-arc basalts and subduction initiation in the Izu–Bonin–Mariana system. *Geochem. Geophys. Geosyst.* 11, 1–17 (2010).
15. Pearce, J. A. & Robinson, P. T. The Troodos ophiolitic complex probably formed in a subduction initiation, slab edge setting. *Gondwana Research* 18(1), 60-81 (2010).
16. Li, Y., Wang, G., Santosh, M., Wang, J., Dong, P., & Li, H. (2020). Subduction initiation of the SE Paleo-Asian Ocean: Evidence from a well preserved intra-oceanic forearc ophiolite fragment in central Inner Mongolia, North China. *Earth and Planetary Science Letters* 535, 116087.
17. Cawood, P.A., & Suhr, G. (1992). Generation and obduction of ophiolites: Constraints from the Bay of Islands Complex, western Newfoundland. *Tectonics* 11(4), 884-897.
18. Bédard, J.H., Lauzière, K., Tremblay, A., & Sangster, A. Evidence from Betts Cove ophiolite boninites for forearc seafloor-spreading: *Tectonophysics* 284, 233–245 (1998).
19. Cawood, P. A., Johnson, M. R., & Nemchin, A. A. Early Palaeozoic orogenesis along the Indian margin of Gondwana: Tectonic response to Gondwana assembly. *Earth and Planetary Science Letters* 255(1-2), 70-84 (2007).
20. Li, S. Z. et al. Closure of the Proto-Tethys Ocean and Early Paleozoic amalgamation of microcontinental blocks in East Asia. *Earth-Science Reviews* 186, 37-75 (2018).
21. Zhao, G. C. et al. Geological reconstructions of the East Asian blocks: From the breakup of Rodinia to the assembly of Pangea. *Earth-Science Reviews* 186, 262-286 (2018).
22. Shu, L.S. et al. Precambrian tectonic evolution of the Tarim Block, NW China: new geochronological insights from the Quruqtagh domain. *Journal of Asian Earth Science* 42, 774–790 (2011).

23. Zhao, G.C. & Cawood, P.A. Precambrian Geology of China. *Precambrian Research* (222–223), 13–54 (2012).
24. Ge, R.F. et al. Generation of Eoarchean continental crust from altered mafic rocks derived from a chondritic mantle: The ~3.72 Ga Aktash gneisses, Tarim Craton (NW China). *Earth and Planetary Science Letters* 538, 116225 (2020).
25. Xiao, W., Windley, B. F., Hao, J. & Li, J. Arc-ophiolite obduction in the Western Kunlun Range (China): implications for the Palaeozoic evolution of central Asia. *Journal of the Geological Society* 159(5), 517-528 (2002).
26. Yin, A. et al. Tectonic history of the Altyn Tagh fault system in northern Tibet inferred from Cenozoic sedimentation. *Geological Society of American. Bulletin* 114, 1257–1295 (2002).
27. Liu, L. et al. Evidence of former stishovite in UHP eclogite from the South Altyn Tagh, western China. *Earth and Planetary Science Letters* 484, 353-362 (2018).
28. Zhang, J. X. et al. Subduction, accretion and closure of Proto-Tethyan Ocean: Early Paleozoic accretion/collision orogeny in the Altun-Qilian-North Qaidam orogenic system. *Acta Petrologica Sinica*, 31(12), 3531-3554 (2015). (in Chinese with English abstract).
29. Zhang, J.X., Yu, S.Y. & Mattinson, C.G. Early Paleozoic polyphase metamorphism in northern Tibet, China. *Gondwana Research* 41, 267-289 (2017).
30. Wang, C. et al. Provenance and ages of the Altyn Complex in Altyn Tagh: implications for the early Neoproterozoic evolution of northwestern China. *Precambrian Research* 230, 193–208 (2013).
31. Cowgill, E., Yin, A., Harrison, T. M., & Xiao-Feng, W. Reconstruction of the Altyn Tagh fault based on U-Pb geochronology: Role of back thrusts, mantle sutures, and heterogeneous crustal strength in forming the Tibetan Plateau. *Journal of Geophysical Research: Solid Earth* 108(B7) (2003).
32. Bureau of Geology and Mineral Resources of Xinjiang Uygur Autonomous Region (BGMRXUAR). Regional Geology of Xingjiang Uyger Autonomous Region. Geological Publishing House, China, pp. 315–318 (in Chinese with English abstract) (1993).
33. Liu, Q. et al. Provenance of early Paleozoic sedimentary rocks in the Altyn Tagh orogen: Insights into the paleoposition of the Tarim craton in northern Gondwana associated with final closure of the Proto− Tethys Ocean. *Geological Society of America Bulletin* (2020).
34. Liu, L., Kang, L., Cao, Y.T. & Yang, W.Q. Early Paleozoic granitic magmatism related to the processes from subduction to collision in South Altyn, NW China. *Science China: Earth Sciences* 58, 1513–1522 (2015).
35. Liu, C. H. et al. Age, composition, and tectonic significance of Palaeozoic granites in the Altyn orogenic belt, China. *International Geology Review* 58(2), 131-154 (2016).
36. Sobel, E. R. & Arnaud, N. A possible middle Paleozoic suture in the Altyn Tagh, NW China. *Tectonics* 18(1), 64-74 (1999).
37. Kang, L. et al. Early Paleozoic magmatism and collision orogenic process of the South Altyn. *Acta Geologica Sinica* 90(10), 2527-2550 (2016).

38. Yang, J. S. et al. Petrology and SHRIMP age of the Hongliugou ophiolite at Milan, north Altun, at the northern margin of the Tibetan plateau. *Acta Petrologica Sinica* 24(7), 1567-1584 (2008) (in Chinese with English abstract).
39. Gao, X., Xiao, P., Guo, L., Dong, Z., & Xi, R. Opening of an early Paleozoic limited oceanic basin in the northern Altyn area: Constraints from plagiogranites in the Hongliugou-Lapeiquan ophiolitic mélange. *Science China–Earth Sciences* 54(12), 1871–1879 (2011).
40. Valley, J.W., Kinny, P.D., Schulze, D.J. & Spicuzza, M.J. Zircon megacrysts from kimberlite: oxygen isotope variability among mantle melts. *Contributions to Mineralogy and Petrology* 133, 1-11 (1998).
41. Condie, K.C. Geochemical changes in basalts and andesites across the Archean-Proterozoic boundary: identification and significance. *Lithos* 23, 1–18 (1989).
42. Reagan, M. K. et al. Petrogenesis of Volcanic Rocks from Saipan and Rota, Mariana Islands, and Implications for the Evolution of Nascent Island Arcs. *Journal of Petrology* 49(3), 441-464 (2008).
43. Sorbadere, F., Schiano, P., Metrich, N. & Bertagnini, A. Small-scale coexistence of island-arc- and enriched-MORB-type basalts in the central Vanuatu arc. *Contributions to Mineralogy and Petrology* 166(5), 1305–1321 (2013).
44. De Hoog, J.C.M. et al. Hydrogen incorporation and charge balance in natural zircon. *Geochimica Et Cosmochimica Acta,* 141, 472-486 (2014).
45. Grimes, C.B. et al. Perspectives on the origin of plagiogranite in ophiolites from oxygen isotopes in zircon. *Lithos* 179, 48-66 (2013).
46. Song, S. G. et al. Continental orogenesis from ocean subduction, continent collision/subduction, to orogen collapse, and orogen recycling: The example of the North Qaidam UHPM belt, NW China. *Earth-Science Reviews* 129, 59-84 (2014).
47. Dong, Y.P. & Santosh, M. Tectonic architecture and multiple orogeny of the Qinling Orogenic Belt, Central China. *Gondwana Research* 29(1), 1-40 (2016).
48. Huang, B., Piper, J. D., Sun, L. & Zhao, Q. New paleomagnetic results for Ordovician and Silurian rocks of the Tarim Block, Northwest China and their paleogeographic implications. *Tectonophysics* 755, 91-108 (2019).
49. Dong, Y. P. et al. Subduction and accretionary tectonics of the East Kunlun orogen, western segment of the Central China Orogenic System. *Earth-Science Reviews* 186, 231-261 (2018).
50. Cawood, P. A., & Buchan, C. Linking accretionary orogenesis with supercontinent assembly. *Earth-Science Reviews* 82(3-4), 217-256 (2007).
51. Herzberg, C., Condie, K. & Korenaga, J. Thermal history of the Earth and its petrological expression: Earth and Planetary Science Letters 292, 79–88 (2010).
52. Brown, M., Kirkland, C.L., & Johnson, T.E. Evolution of geodynamics since the Archean: Significant change at the dawn of the Phanerozoic. *Geology* 48, 488–492 (2020).
53. Bono, R. K., Tarduno, J. A., Nimmo, F., & Cottrell, R. D. Young inner core inferred from ediacaran ultra-low geomagnetic field intensity. *Nature Geoscience* 12, 143–147 (2019).

54. Sun, S. S., & McDonough, W. F. Chemical and isotopic systematics of oceanic basalts: implications for mantle composition and processes. *Geological Society, London, Special Publications 42(1)*, 313-345 (1989).
55. McDonough, W. F., & Sun, S. S. The composition of the Earth. *Chemical geology* 120(3-4), 223-253 (1995).
56. Uysal, I. et al. Coexistence of abyssal and ultra-depleted SSZ type mantle peridotites in a Neo-Tethyan Ophiolite in SW Turkey: Constraints from mineral composition, whole-rock geochemistry (major–trace–REE–PGE), and Re–Os isotope systematics. *Lithos* 132-133, 50-69 (2012).
57. Gray, D.R. et al. A Damara orogen perspective on the assembly of southwestern Gondwana. In: Pankhurst, R.J., Trouw, R.A.J., Brito Neves, B.B., de Wit, M.J. (Eds.), West Gondwana: Pre-Cenozoic Correlations Across the South Atlantic Region. 294. *Geological Society, London, Special Publications*, 257–278 (2008).
58. Schmitt, R.S., Fragoso, R.A. & Collins, A.S. Suturing Gondwana in the Cambrian: the orogenic events of the final amalgamation. *In: Geology of Southwest Gondwana–Regional Geology Reviews, 1 ed. Springer International Publishing*, pp. 63–85 (2018).

Figures

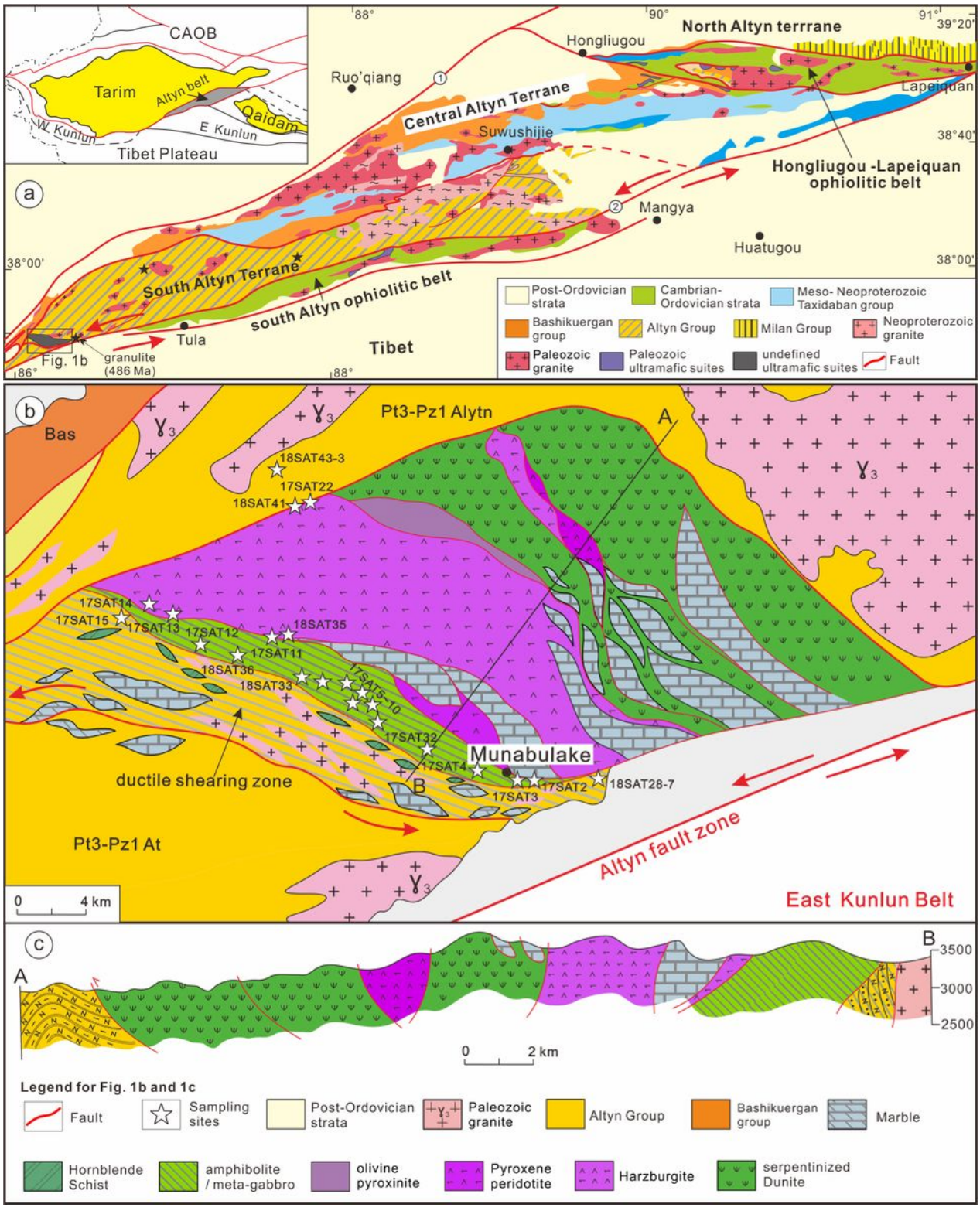

Figure 1

a) Geological sketch map of the Altyn Belt; b) Geological map of the Munabulake ophiolite; c) Regional cross section of the Munabulake ophiolite.

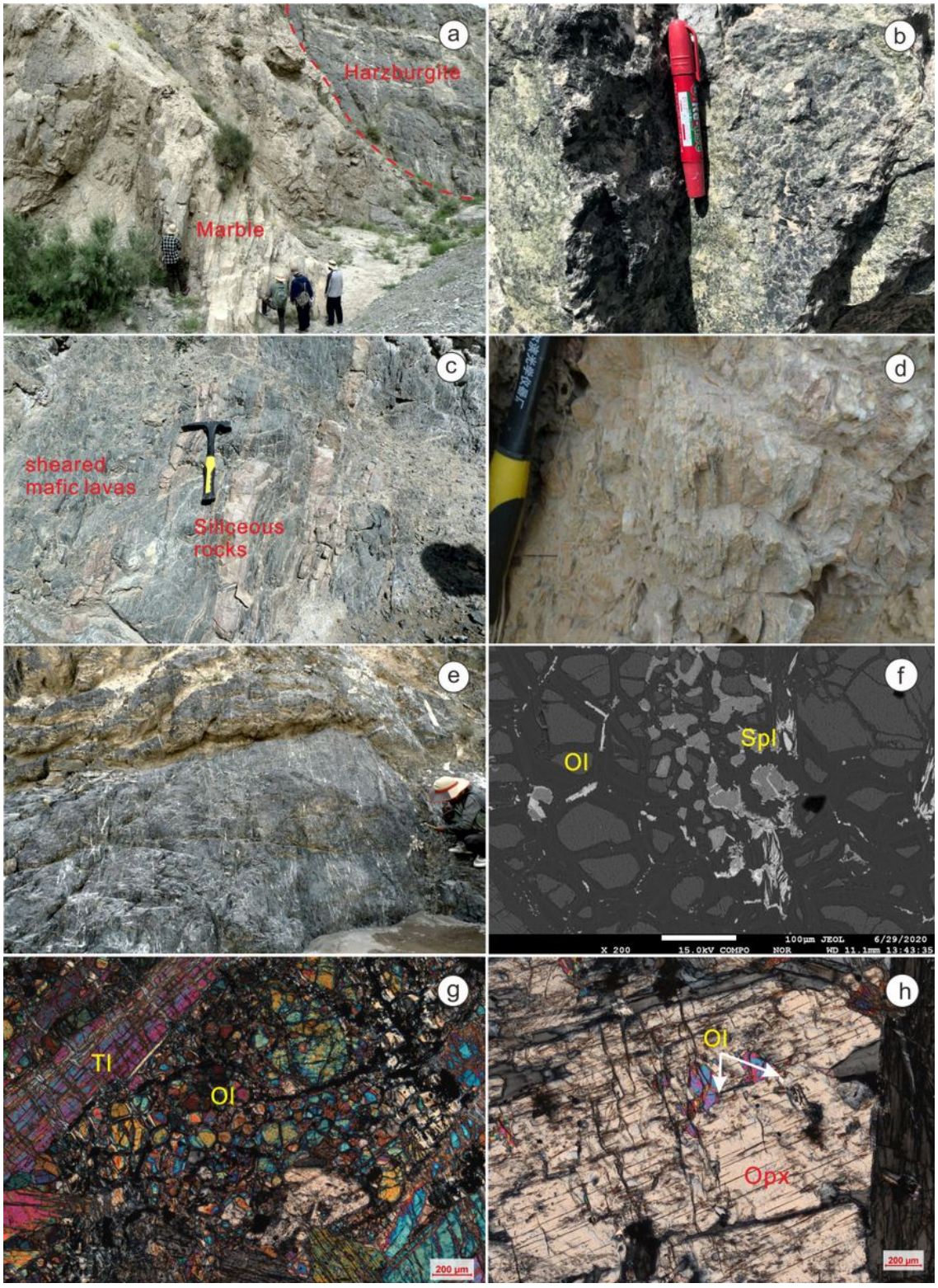

Figure 2

Representative field photos of the Munabulake ophiolite, and thin-section photomicrographs and BSE (Electron back scattered diffraction) image of samples, (a) marble blocks within harzburgite; (b) harzburgite; (c) blocks of siliceous rocks within meta-mafic lavas; (d) siliceous rocks of varied thickness interlayered with sheared mafic lavas; (e) meta-mafic lavas; (f) spinel in harzburgite; (g) Tremolite and

olivine within olivine pyroxenite; (h) olivine with serpentinized rims observed in harzburgite. Abbreviations: Ol, olivine; Opx, orthopyroxene; Sp, spinel; Tl, tremolite.

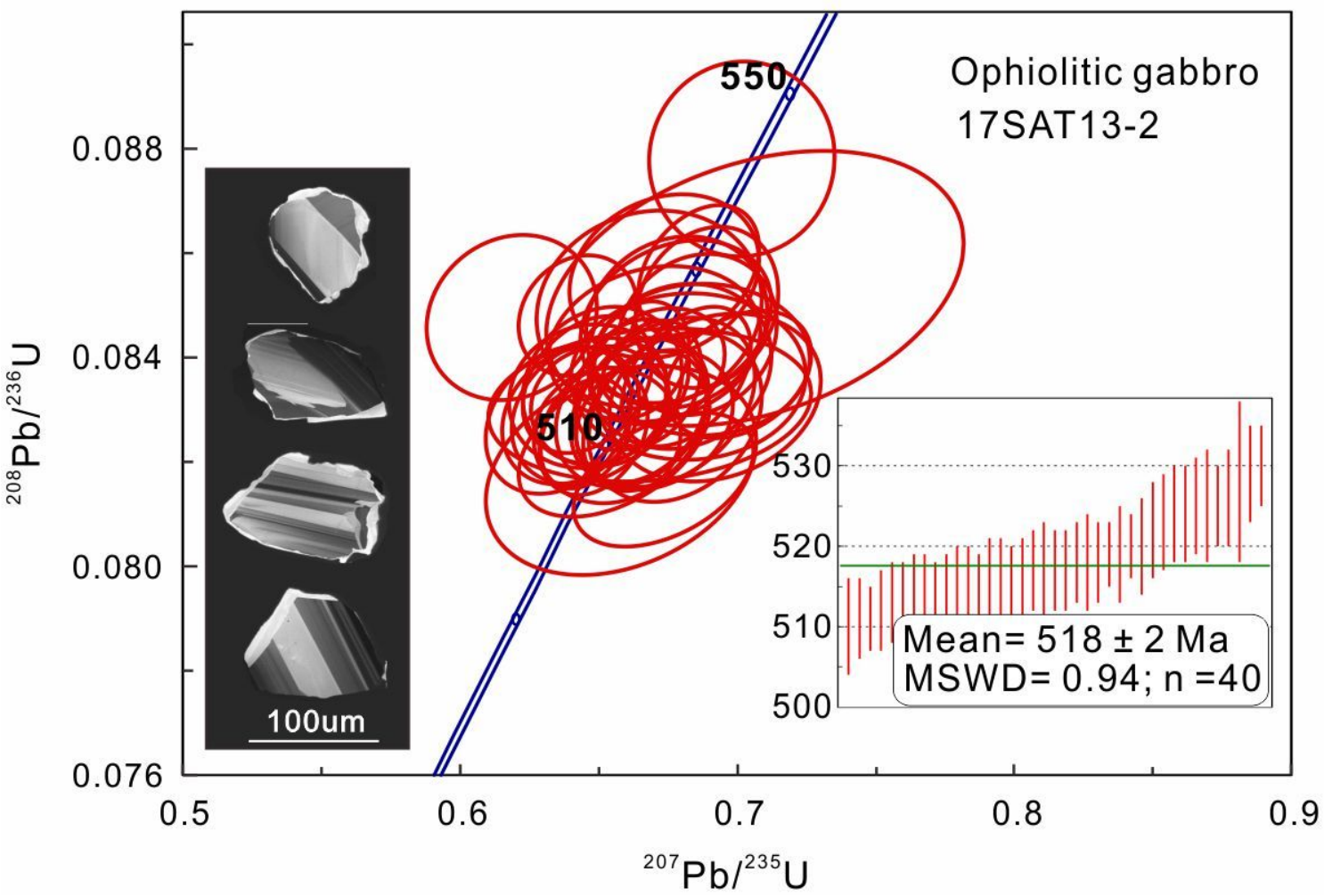

Figure 3

U-Pb concordia plots for zircons from ophiolitic gabbro 17SAT13-2

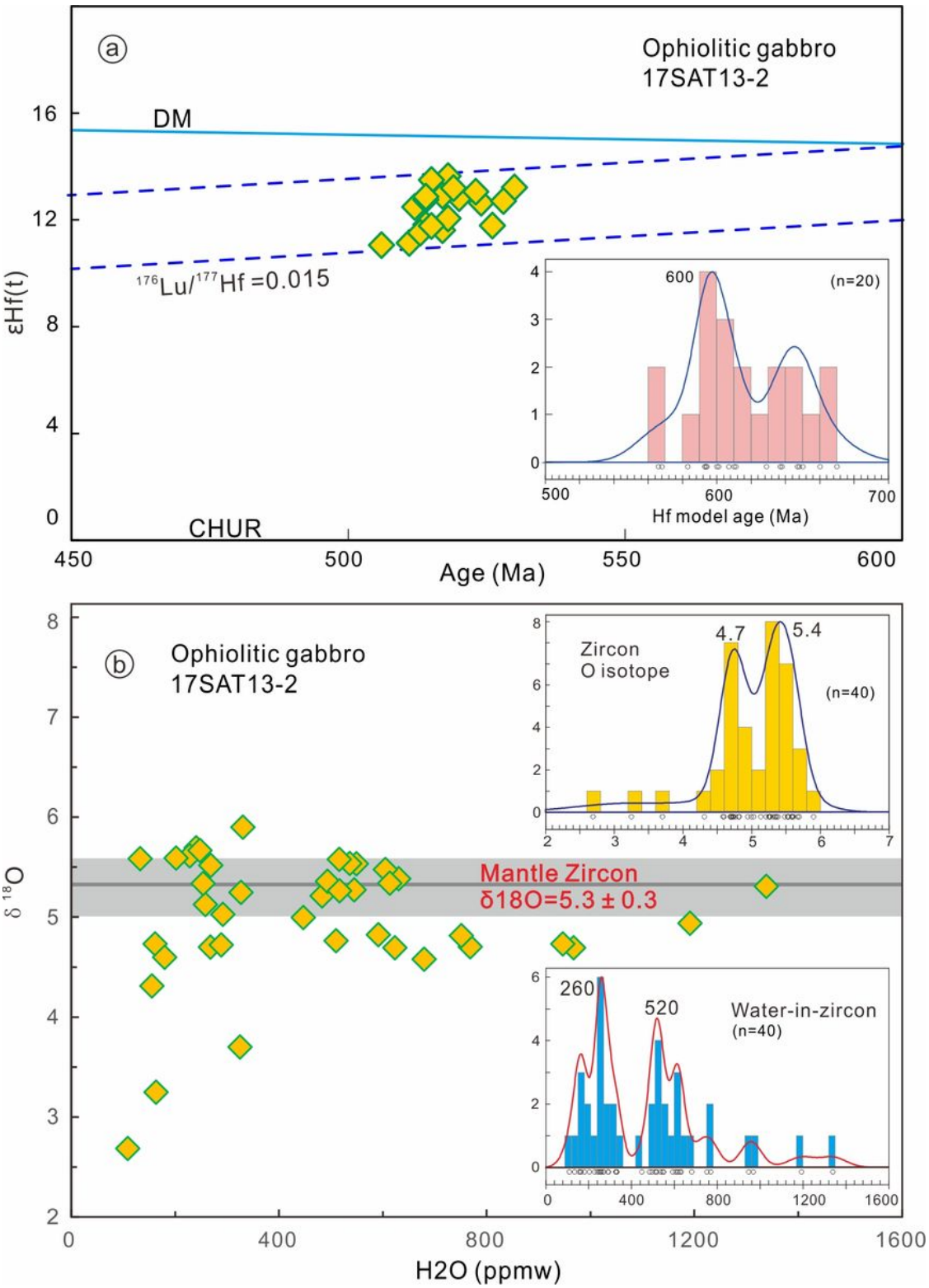

Figure 4

(a) Hf isotopes and (b) δ18O versus H2O content for zircons from ophiolitic gabbro 17SAT13-2.

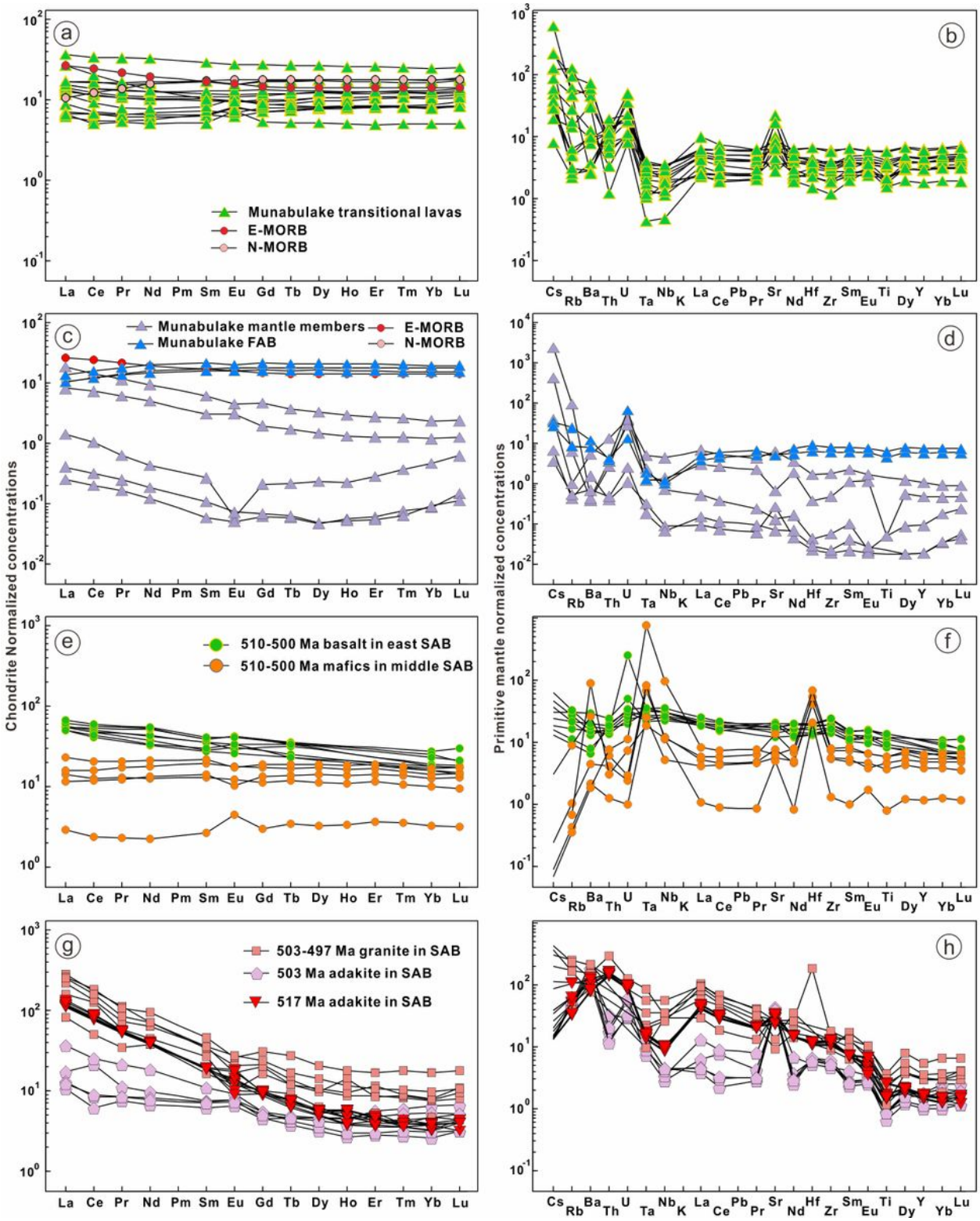

Figure 5

Chondrite normalized REE patterns for (a) transitional lavas of the Munabulake ophiolite; (c) fore-arc basalt and residue mantle member samples of the Munabulake ophiolite. Primitive mantle– normalized incompatible element distribution spidergrams for (b) transitional lavas of the Munabulake ophiolite; (d) fore-arc basalt and residue mantle member samples of the Munabulake ophiolite; (e) REE patterns and (f) incompatible element distribution spidergrams for MORB type mafic-ultramafic suites in the South Altyn

ophiolite belt; (g) REE patterns and (f) incompatible element distribution spidergrams for adakites and calc-alkaline granitoids within the South Altyn ophiolite belt. (The normalization values are from 54-55). Abbreviations: SAB, South Altyn ophiolite belt.

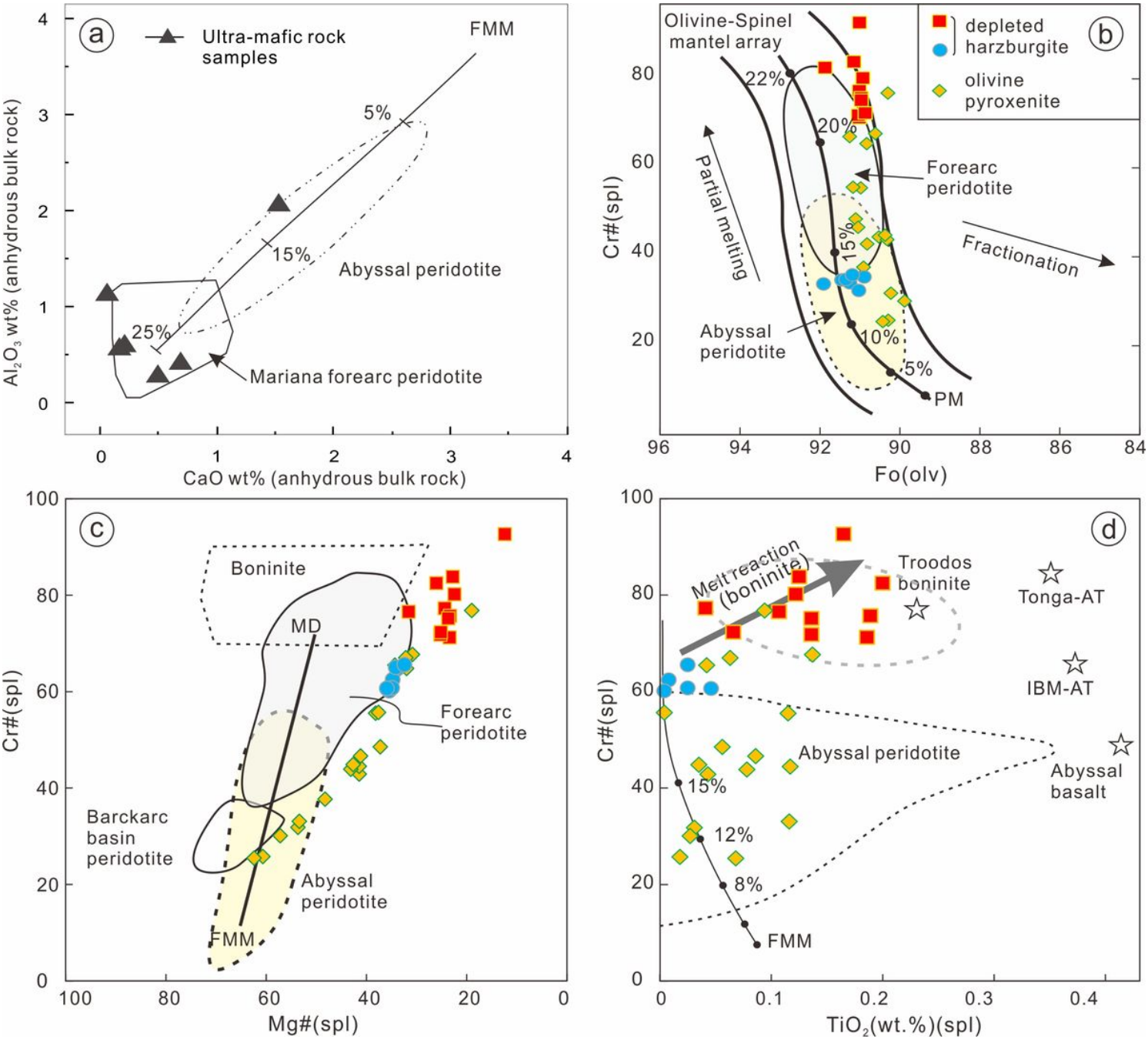

Figure 6

(a) Bulk-rock abundances of Al2O3 versus CaO (volatile free, normalized to 100% total), showing how melting depletes peridotites in these elements; (b) Cr# (Cr/Cr + Al) versus Mg# (Mg/Mg + Fe+2) diagram for composition of spinels in peridotite; (c) compositional relationship between Cr# of spinel and Fo [100 Mg/(Mg+Fe2+)] content of coexisting olivine in peridotite samples; (d) compositional variations of Cr# vs. TiO2 (wt.%) content of spinels in peridotite samples of the Munabulake ophiolite. Fields for passive margin, abyssal and forearc peridotites and degrees of melt extractions can be found in 12, 56 and

references therein. Abbreviations: FMM: Fertile midocean-ridge basalt (MORB)–type mantle; PM: Primitive Mantle.

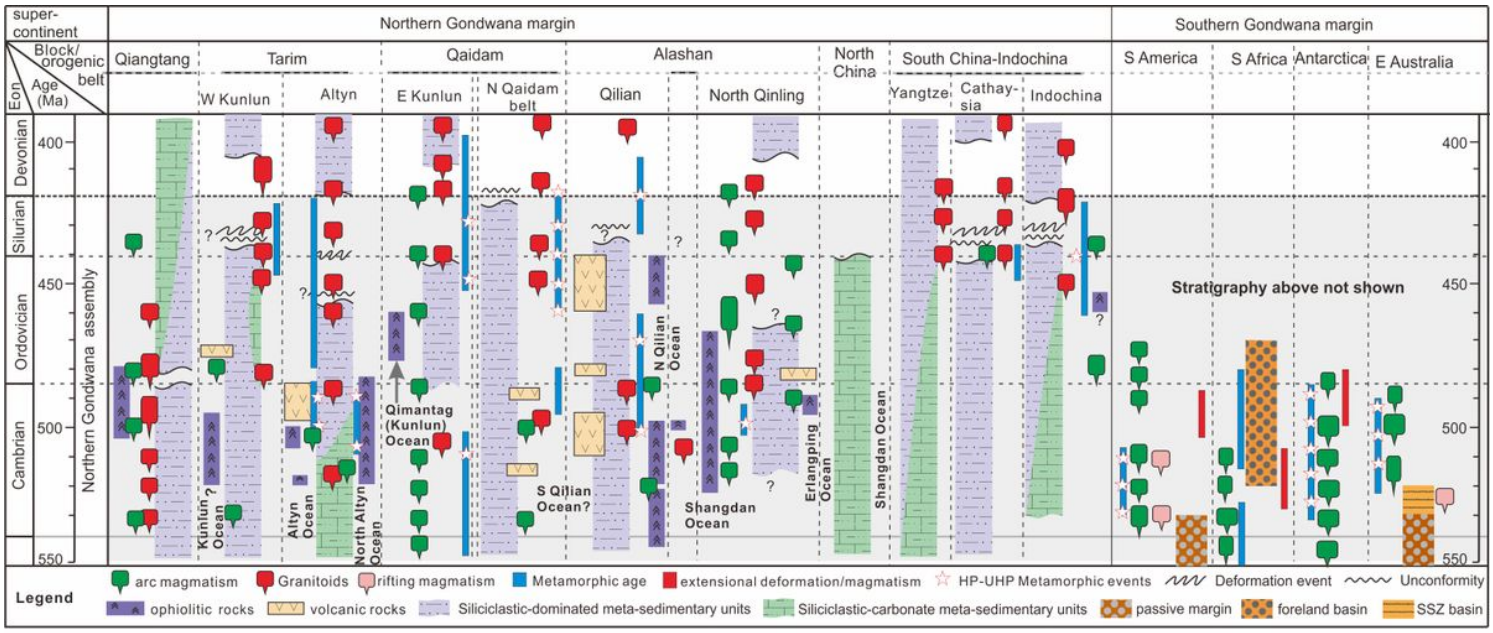

Figure 7

Time-space plot for the early Paleozoic sequences, ophiolites, stratigraphic sequences and metamorphic events in Proto-Tethys and Pacific margins of Gondwana. The complete list of references for age data points are given in the supplementary material.

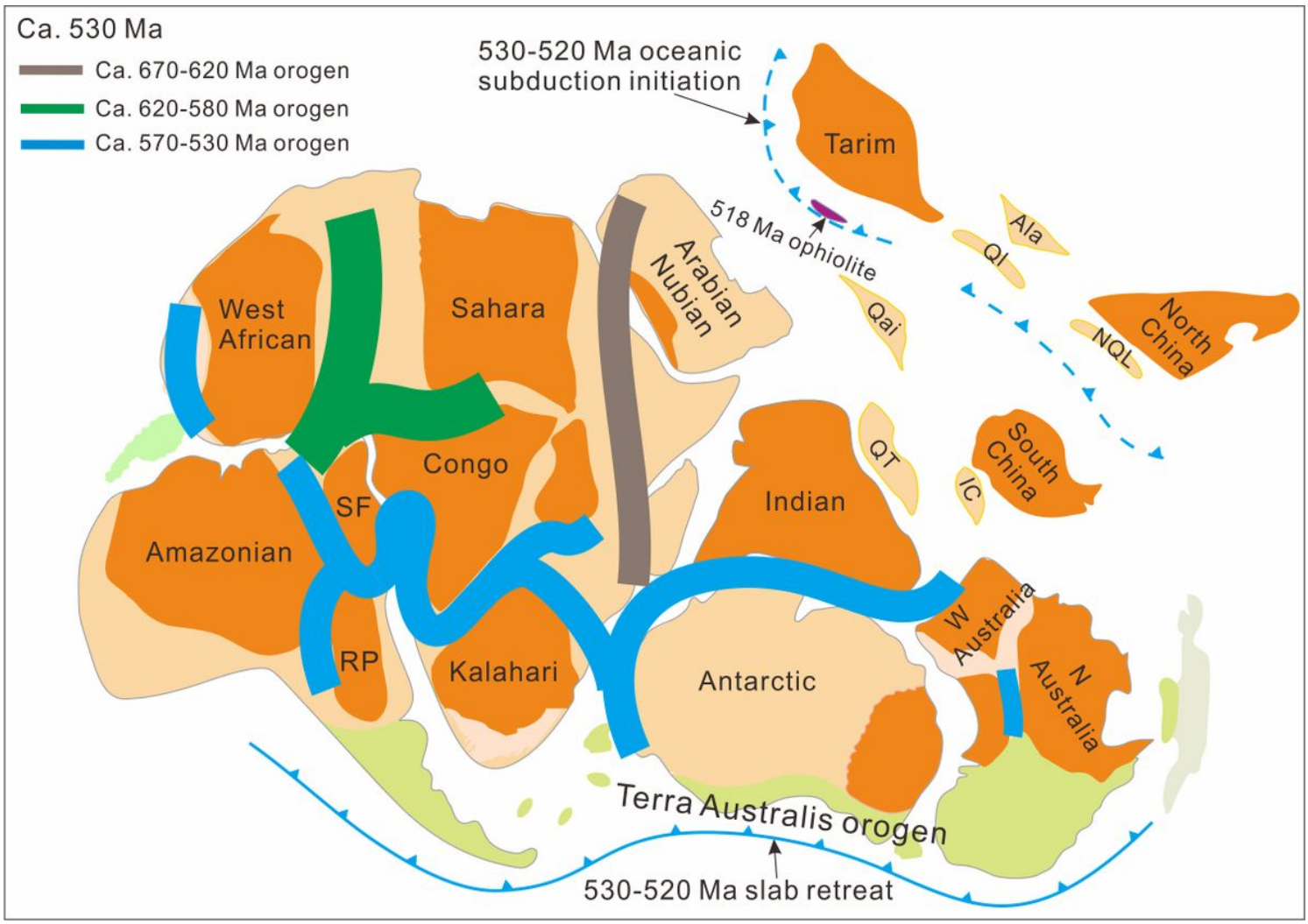

Figure 8

Reconstruction of Gondwana and subduction zones in its southern and northern margins (revised based on 21, 50, 57-58).

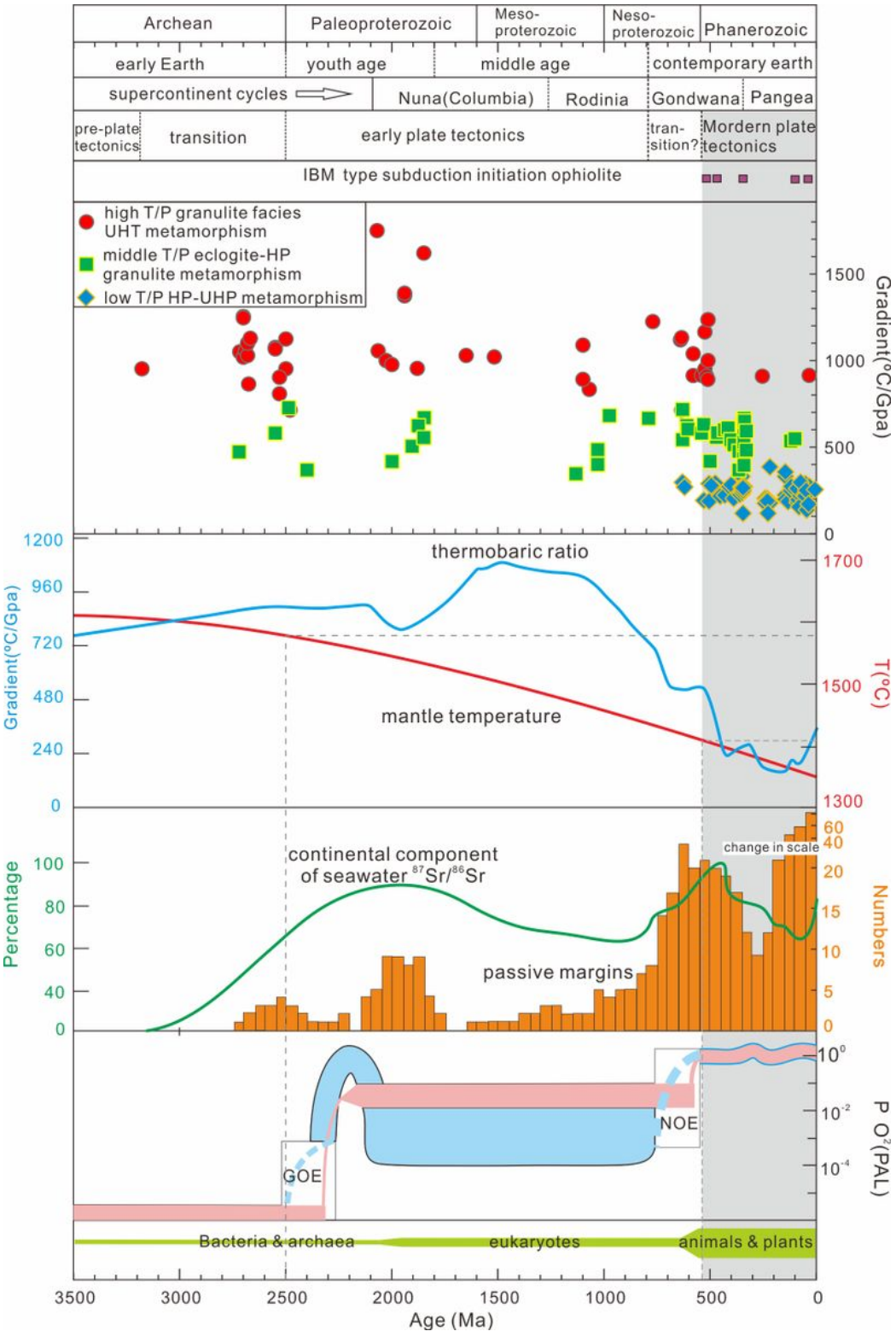

Figure 9

Stages of geodynamic regimes with respect to ages of subduction initiation ophiolites, thermal gradient versus metamorphic ages of three main types of granulite facies metamorphism, thermobaric ratio curve, the inferred mantle potential temperature, the normalized seawater 87Sr/86Sr curve, the ages of ancient and modern passive margins, the changing oxygen levels within the atmosphere relative to present

atmospheric level and the evolution of life within the biosphere (after 3,8 and references therein). Gray shaded bar corresponds to the Phanerozoic time.

Supplementary Files

This is a list of supplementary files associated with this preprint. Click to download.

- SupportingdataandDataAvailabilityStatement.docx